Check for updates

Proceedings of the ASME 2018 International Design Engineering Technical Conferences and Computers and Information in Engineering Conference
IDETC/CIE 2018
August 26-29, 2018, Quebec City, Quebec, Canada

DETC2018-85232

Downloaded from https://asmedigitalcollection.asme.org/IDETC-CIE/proceedings-pdf/IDETC-CIE2018/51838/V006T09A015/2476548/v006t09a015-detc2018-85232.pdf by McGill University user on 08 October 2019

A UNIT-CONSISTENT ERROR MEASURE FOR MIXED LINEAR COMPLEMENTARITY PROBLEMS IN MULTIBODY DYNAMICS WITH CONTACT

Andreas Enzenhöfer*
Department of Mechanical Engineering
Centre for Intelligent Machines
McGill University
Montreal, Quebec, H3A 2T5, Canada
Email: andreas.enzenhofer@mail.mcgill.ca

Albert Peiret
Department of Mechanical Engineering
Centre for Intelligent Machines
McGill University
Montreal, Quebec, H3A 2T5, Canada
Email: albert.peiret@mail.mcgill.ca

Marek Teichmann
CM Labs Simulations Inc.
Montreal, Quebec, H3C 1T2, Canada
Email: marek@cm-labs.com

József Kövecses
Department of Mechanical Engineering
Centre for Intelligent Machines
McGill University
Montreal, Quebec, H3A 2T5, Canada
Email: jozsef.kovecses@mcgill.ca

ABSTRACT

Modeling multibody systems subject to unilateral contacts and friction efficiently is challenging, and dynamic formulations based on the mixed linear complementarity problem (MLCP) are commonly used for this purpose. The accuracy of the MLCP solution method can be evaluated by determining the error introduced by it. In this paper, we find that commonly used MLCP error measures suffer from unit inconsistency leading to the error lacking any physical meaning. We propose a unit-consistent error measure which computes energy error components for each constraint dependent on the inverse effective mass and compliance. It is shown by means of a simple example that the unit consistency issue does not occur using this proposed error measure. Simulation results confirm that the error decreases with convergence toward the solution. If a pivoting algorithm does not find a solution of the MLCP due to an iteration limit, e.g. in real-time simulations, choosing the result with the least error can reduce the risk of simulation instabilities.

INTRODUCTION

There are numerous issues that make multibody dynamics simulations with contacts and friction challenging. Many applications in engineering and related fields impose strict requirements on the computational time available for each time step and on the accuracy of the simulation, such as in real-time simulations. Accurate solutions and low computational time usually cannot be obtained simultaneously. Contact in multibody systems can be modeled through unilateral constraints. This often results in a dynamic formulation that can mathematically be described as a *linear complementarity problem* (LCP) or *mixed linear complementarity problem* (MLCP). There is a wide range of algorithms in the literature to solve LCPs and MLCPs, which can be classified into two types: direct and iterative methods [1]. Generally, iterative solvers are computationally more efficient than direct ones. Nevertheless, only direct solvers are able to deliver the exact solution of the MLCP given enough computational time.

It is not an easy task to choose the solver that best suits the

*Address all correspondence to this author.

Copyright © 2018 ASME

problem at hand, especially when there is a time constraint and a solution with the desired tolerance cannot be found. In this case, the simulation accuracy can be increased significantly if we measure the error of all computed solutions throughout the solver iterations and choose the solution with the least error. In this paper, we introduce two commonly used error measures such as the natural residual [2] and the Fischer-Burmeister function [3] and show that these approaches do not take the nature of the model into account and can suffer from physical inconsistency. Furthermore, we present a unit-consistent energy error measure for MLCP solvers that does not require any reference solution and can be efficiently computed for every solver iteration in order to improve simulation accuracy.

RELATED WORK

The mathematics literature contains many papers and books about the theory of error bounds on the complementarity problem (CP), i.e. the general problem formulation containing the LCP, MLCP and nonlinear complementarity problem (NCP). Pang [2, 4] defines the natural residual as the componentwise minimum between the CP solution vector and the slack vector. This residual can be used to measure the closeness of the computed result to being a solution of the CP. Fukushima [3] discusses several merit functions one of which is the Fischer-Burmeister function. This function is defined by the componentwise difference between the ℓ_2-norm and the ℓ_1-norm of two components of the solution and slack vector. The Fischer-Burmeister merit function is commonly used to capture the error in rigid body simulations [5, 6]. Lu and Trinkle [7] measure the error in a potential solution using the Chen-Chen-Kanzow reformulation function which also depends on the Fischer-Burmeister function. Lacoursière et al. [8] introduce multiple quality metrics which do not only measure the MLCP solver error but also the penetration error as well as the error in the friction force magnitude and alignment. It is not in the scope of this present paper to determine and evaluate the error in the dynamic formulation, it measures the MLCP solver error only.

The great advantage of the presented residual and merit functions for the CP is that the CP conditions are used to determine the error in the computed result so that no reference solution is required. Furthermore, the error can be computed relatively inexpensively in every algorithm iteration. This is advantageous because we can keep track of the solver error throughout the iterations so that the solution with the least error can be chosen in case the solver does not terminate due to an iteration limit. However, these error functions have a major drawback if used for mechanical problems. They do not take the physical nature of the solution vector (forces or impulses) and the slack vector (accelerations or velocities) into consideration. Thus, the computed errors are unit inconsistent and have no physical meaning.

MULTIBODY DYNAMICS WITH CONTACT

Let us consider a multibody system with the generalized velocities $\mathbf{v} \in \mathbb{R}^{6m}$ for m rigid bodies and the transformation $\mathbf{J}\mathbf{v} = \mathbf{w}$ that defines the constraint subspace where $\mathbf{w} \in \mathbb{R}^n$ represents the velocities in that subspace and $\mathbf{J} \in \mathbb{R}^{n\times 6m}$ is the constraint Jacobian. The dynamic equations using a finite difference approximation for the generalized accelerations $\dot{\mathbf{v}} \approx \frac{\mathbf{v}^+ - \mathbf{v}}{h}$ and constraint regularization can be written as [9]

$$\begin{bmatrix} \mathbf{M} & -\mathbf{J}^{\mathrm{T}} \\ \mathbf{J} & \mathbf{C} \end{bmatrix} \begin{bmatrix} \mathbf{v}^+ \\ h\boldsymbol{\lambda}^+ \end{bmatrix} + \begin{bmatrix} \mathbf{p} \\ \frac{1}{h}\boldsymbol{\Phi} \end{bmatrix} = \begin{bmatrix} \mathbf{0} \\ \mathbf{w} \end{bmatrix} \tag{1}$$

where h is the time step size, $\mathbf{v}^+$ are the unknown velocities at the end of the step, $\mathbf{v}$ are the known velocities at the beginning of the step, $\mathbf{M} \in \mathbb{R}^{6m\times 6m}$ is the mass matrix, and $\mathbf{p} = \mathbf{M}\mathbf{v} + h\mathbf{f}_a \in \mathbb{R}^m$ combines the momentum and impulse dependent on the generalized applied forces $\mathbf{f}_a$. The limits on the constraint reactions $\boldsymbol{\lambda}^+ \in \mathbb{R}^n$ are specified by the nature of the constraint, e.g. $\lambda_{\mathrm{n}}^+ \geq 0$ for a normal contact force, and $\lambda_{\mathrm{t}}^+ \in [-\mu\lambda_{\mathrm{n}}, +\mu\lambda_{\mathrm{n}}]$ for a friction force component if the box friction approximation is used, where λ_n can be an estimate of the normal force from the previous time step [9]. Moreover, the constraints can be regularized through representation of the reaction forces by constitutive relations in implicit form, i.e. $\lambda_i^+ = -k_i\phi_i^+$, where k_i is the constraint stiffness and ϕ_i^+ is the constraint violation at the end of the time step. This introduces the compliance matrix $\mathbf{C} = \mathrm{diag}\{\frac{1}{k_1 h^2}, \ldots, \frac{1}{k_n h^2}\} \in \mathbb{R}^{n\times n}$ and the constraint violation vector $\boldsymbol{\Phi} = [\phi_1, \ldots, \phi_n]^{\mathrm{T}} \in \mathbb{R}^n$. Note that the constraint violations of the next time-step are approximated via a finite difference, so that the constraint reactions are defined in terms of the unknown velocities. This makes the constraint forces implicit and adds damping to the system, which increases the stability of the formulation.

Mixed Linear Complementarity Problem

The general form of the MLCP that needs to be solved at each step is

$$\mathbf{A}\mathbf{x} + \mathbf{b} = \mathbf{w}, \tag{2}$$

$$\mathbf{0} \leq \mathbf{u} - \mathbf{x} \perp \mathbf{w}_- \geq \mathbf{0}, \tag{3}$$

$$\mathbf{0} \leq \mathbf{x} - \boldsymbol{l} \perp \mathbf{w}_+ \geq \mathbf{0}, \tag{4}$$

where $\mathbf{A} = \mathbf{J}\mathbf{M}^{-1}\mathbf{J}^{\mathrm{T}} + \mathbf{C}$ is the lead matrix, $\mathbf{b} = \mathbf{J}\mathbf{M}^{-1}\mathbf{p} + \frac{1}{h}\boldsymbol{\Phi}$ is called parameter vector, and the variables $\mathbf{x} = h\boldsymbol{\lambda}^+ \in [\boldsymbol{l}, \mathbf{u}]$ are the constraint impulses subject to lower and upper bounds $\boldsymbol{l}$ and $\mathbf{u}$. The nonnegative components of the constraint-space velocity (also known as slack variables) $\mathbf{w} = \mathbf{w}_+ - \mathbf{w}_-$ are complementary to the saturation of the lower and upper bounds, denoted by the operator $\perp$. Therefore, the slack variable is positive ($w_{+,i} > 0$) when the main variable x_i is at the lower bound

Downloaded from https://asmedigitalcollection.asme.org/IDETC-CIE/proceedings-pdf/IDETC-CIE2018/51838/V006T09A015/2476548/v006009a015-detc2018-85232.pdf by McGill University user on 08 October 2019

Copyright © 2018 ASME

($x_i = l_i$). Likewise, the slack variable is negative ($w_{-,i} > 0$) when the main variable x_i is at the upper bound ($x_i = u_i$).

Solver Algorithms

There are two main types of algorithms for solving an MLCP: *direct* and *indirect* methods [1]. Direct methods, also known as *pivoting methods*, try to determine the set of variables that are at the upper or lower bound, or within the bounds. They start with an initial guess for these index sets in order to solve for the unknown variables. If the guess does not lead to a solution of the MLCP, the index sets are modified by systematically swapping variables from one set to another until a solution is reached. Unfortunately, there is no guarantee that the result in an iteration is closer to the solution than the previous result.

In contrast to direct methods, indirect or *iterative* methods do not make assumptions on index sets nor solve directly for the unknown variables. Instead, convergence is reached by improving the solution of the previous iteration so that the obtained solution of the next iterate is closer than the previous if the solver is convergent for the problem at hand. In order to solve the MLCP, direct and iterative solution algorithms perform a series of iterations and compute intermediate solutions, which satisfy Eq. (2) so that the solver error occurs only in the conditions in Eqs. (3) and (4).

EXISTING ERROR MEASURES

In the following sections, we present two functions that can be used to measure the solver error per constraint based on the MLCP solution $\mathbf{x}$ and slack variable $\mathbf{w}$. If Eq. (2) is satisfied, the variable x_i represents the constraint reaction impulse, and its slack variable w_i represents the constraint velocity. However, for an intermediate solution before the algorithm converges, the feasibility of the impulses ($x_i \in [l_i, u_i]$) or the complementarity of the slack variables may not be guaranteed.

Fischer-Burmeister Error Function

For the MLCP in Eqs. (2) to (4), two Fischer-Burmeister error functions are introduced per constraint i [3, 10]

$$\begin{aligned} \phi_{\mathrm{FB},u,i} &= (u_i - x_i) + w_{-,i} - \sqrt{(u_i - x_i)^2 + w_{-,i}^2}, \\ \phi_{\mathrm{FB},l,i} &= (x_i - l_i) + w_{+,i} - \sqrt{(x_i - l_i)^2 + w_{+,i}^2}. \end{aligned} \tag{5}$$

We take the maximum of the absolute values resulting from Eq. (5) to obtain one error value for constraint i

$$\delta\phi_{\mathrm{FB},i} = \max\left(|\phi_{\mathrm{FB},l,i}|, |\phi_{\mathrm{FB},u,i}|\right). \tag{6}$$

Given $\delta\phi_{\mathrm{FB},i}$, we can compute an error value for the entire system of equations, called *system error*. The ℓ_1-norm of the component vector $\delta\boldsymbol{\phi}_{\mathrm{FB}} = [\delta\phi_{\mathrm{FB},1} \dots \delta\phi_{\mathrm{FB},n}]^{\mathrm{T}}$ can be used to define the system error as

$$\delta\phi_{\mathrm{FB}} = ||\delta\boldsymbol{\phi}_{\mathrm{FB}}||_1 = \sum_{i=1}^{n} |\delta\phi_{\mathrm{FB},i}|. \tag{7}$$

Natural Residual

Similar to the approach for the Fischer-Burmeister function, we can introduce two natural residuals per constraint i for an MLCP [2, 4]

$$\begin{aligned} \phi_{\mathrm{res},u,i} &= \min\left(u_i - x_i, w_{-,i}\right), \\ \phi_{\mathrm{res},l,i} &= \min\left(x_i - l_i, w_{+,i}\right), \end{aligned} \tag{8}$$

where the arguments in the minimum function represent the variables in the conditions in Eqs. (3) and (4). We define the error of constraint i as the maximum of the absolute values of the two functions in Eq. (8)

$$\delta\phi_{\mathrm{res},i} = \max\left(|\phi_{\mathrm{res},u,i}|, |\phi_{\mathrm{res},l,i}|\right). \tag{9}$$

The system error can then be defined using the ℓ_1-norm

$$\delta\phi_{\mathrm{res}} = ||\delta\boldsymbol{\phi}_{\mathrm{res}}||_1 = \sum_{i=1}^{n} |\delta\phi_{\mathrm{res},i}|, \tag{10}$$

where $\delta\boldsymbol{\phi}_{\mathrm{res}} = [\delta\phi_{\mathrm{res},1} \dots \delta\phi_{\mathrm{res},n}]^{\mathrm{T}}$ is the component vector composed of the errors for all constraints in the system.

Unit Consistency Issues

The two error measures presented above are commonly used in simulation of multibody systems with contact to estimate the accuracy of the solver algorithm [10, 11]. However, these error measures have a significant shortcoming which is rarely discussed. The different physical nature of the constraint impulses $\mathbf{x}$ and the constraint-space velocities $\mathbf{w}$ are not taken into account. This can lead to unit inconsistencies in the Fischer-Burmeister function. For example, if $u_i - x_i$ and $w_{-,i}$ are simultaneously nonzero, we add impulses expressed in [Ns] to velocities expressed in $\left[\frac{\mathrm{m}}{\mathrm{s}}\right]$ which leads to a sum in Eq. (5) without any physical meaning. Unit inconsistencies in the ℓ_1-norm of the natural residual can also occur if the components of $\delta\boldsymbol{\phi}_{\mathrm{res}}$ contain variables of mixed physical quantities, e.g. impulses expressed in [Ns] and velocities expressed in $\left[\frac{\mathrm{m}}{\mathrm{s}}\right]$. Furthermore, another

Downloaded from https://asmedigitalcollection.asme.org/IDETC-CIE/proceedings-pdf/IDETC-CIE2018/51838/V006T09A015/2476548/v006t09a015-detc2018-85232.pdf by McGill University user on 08 October 2019

Copyright © 2018 ASME

type of unit inconsistency is possible when the constraint velocities $\mathbf{w}$ also represent angular velocities of rigid bodies. Then, $\mathbf{w}$ is composed of a mix of point velocities in $\left[\frac{\mathrm{m}}{\mathrm{s}}\right]$ and angular velocities in $\left[\frac{1}{\mathrm{s}}\right]$. There is no clear physical meaning of the ℓ_1-norm of $\delta\boldsymbol{\phi}_{\mathrm{res}}$ that mixes impulses, point velocities and angular velocities. Even if all error is in the forces, i.e. the components of $\delta\boldsymbol{\phi}_{\mathrm{res}}$ carry exclusively force units, the effect of such force error on the system motion is dependent on the mass of the constrained bodies. For example, a relatively small force error of 10^{-1} N may have a more significant impact on the motion of a light body than a relatively large force error of 10^3 N on the motion of a heavy body.

UNIT-CONSISTENT ERROR MEASURE

In this section, we present a novel error measure that defines the solver error as a function of the MLCP solution vector $\mathbf{x}$ and the slack vector $\mathbf{w}$. This error measure is unit consistent in all the critical scenarios outlined in the previous section, and it is based on constraint error components expressed in energy units, which allows us to easily combine and compare them.

Inverse Effective Mass of a Constraint

We consider a system of m rigid bodies connected by n bilateral and unilateral constraints. The system mass matrix is given by $\mathbf{M} \in \mathbb{R}^{6m\times 6m}$ and the system constraint Jacobian by $\mathbf{J} \in \mathbb{R}^{n\times 6m}$ where the Jacobian row $\mathbf{J}_i \in \mathbb{R}^{1\times 6m}$ corresponds to constraint i. The *effective mass* $m_{\mathrm{eff},i}$ associated with constraint i can be defined as [12, 13]

$$m_{\mathrm{eff},i} = \frac{1}{\mathbf{J}_i\mathbf{M}^{-1}\mathbf{J}_i^{\mathrm{T}}}. \tag{11}$$

This definition of the effective mass is an approximation since only the mass and inertia effects of directly adjacent bodies are taken into consideration and no other constraints between these bodies are regarded. For a long chain of bodies connected by spherical joints, the effective mass of a constraint only contains contributions of the two bodies which are linked to each other by the constraint. For two bodies connected by multiple constraints, e.g. a cube in contact with a plane, the effective mass of constraint 1 does not receive any contribution of constraint 2 even if the same bodies are involved. These approximations have been made to keep the computational cost low so that the solver error can be computed in every iteration without significant impact on the solver performance.

The MLCP lead matrix $\mathbf{A}$ for the box friction model is defined as the sum of the inverse effective mass matrix $\mathbf{J}\mathbf{M}^{-1}\mathbf{J}^{\mathrm{T}}$ and the diagonal regularization matrix $\mathbf{C}$. Then, any diagonal element a_{ii} of $\mathbf{A}$ is simply the sum of the inverse of the effective mass $m_{\mathrm{eff},i}$ and the element c_i of $\mathbf{C}$

$$a_{ii} = \frac{1}{m_{\mathrm{eff},i}} + c_i, \tag{12}$$

where element c_i is the compliance of constraint i. The element a_{ii} combines the inverse of the effective mass with the constraint compliance. It carries inverse mass units $[\mathrm{kg}^{-1}]$ if the translational motion is constrained or inverse inertia units $[(\mathrm{kg\,m}^2)^{-1}]$ if the angular motion is restricted by constraint i. In the following sections, a_{ii} will simply be referred to as *inverse effective mass* element and is given without any additional computations as a diagonal element of $\mathbf{A}$.

Energy Error Measure

Given a solution $\mathbf{x}$ of the MLCP problem in Eq. (2), the i-th component can be decomposed into

$$x_i = x_{0,i} + \delta x_{u,i} - \delta x_{l,i} \tag{13}$$

where the feasible component $x_{0,i} \in [l_i, u_i]$. The other components are defined as

$$\begin{aligned} \delta x_{u,i} &= \max\left(x_i - u_i, 0\right), \\ \delta x_{l,i} &= \max\left(l_i - x_i, 0\right), \end{aligned} \tag{14}$$

which quantify violation of the upper and lower bounds, respectively. On the other hand, the slack variable $\mathbf{w} = \mathbf{A}\mathbf{x} + \mathbf{b}$ is decomposed in the two nonnegative components as

$$w_i = w_{+,i} - w_{-,i}, \tag{15}$$

where $w_{+,i} \geq 0$ and $w_{-,i} \geq 0$.

We define the upper impulse energy error $\delta e_{x_u,i}$, the lower impulse energy error $\delta e_{x_l,i}$, the positive velocity energy error $\delta e_{w_+,i}$, and the negative velocity energy error $\delta e_{w_-,i}$ as

$$\delta e_{x_u,i} = \frac{1}{2} a_{ii} \delta x_{u,i}^2, \tag{16}$$

$$\delta e_{x_l,i} = \frac{1}{2} a_{ii} \delta x_{l,i}^2, \tag{17}$$

$$\delta e_{w_+,i} = \min\left(\frac{1}{2a_{ii}} w_{+,i}^2, \frac{1}{2} a_{ii} \sigma_{l,i}^2\right), \tag{18}$$

$$\delta e_{w_-,i} = \min\left(\frac{1}{2a_{ii}} w_{-,i}^2, \frac{1}{2} a_{ii} \sigma_{u,i}^2\right), \tag{19}$$

where $\sigma_{u,i} = u_i - (x_{0,i} - \delta x_{l,i})$ and $\sigma_{l,i} = (x_{0,i} + \delta x_{u,i}) - l_i$ represent the saturation of the upper and lower bound, respectively.

Downloaded from https://asmedigitalcollection.asme.org/IDETC-CIE/proceedings-pdf/IDETC-CIE2018/51838/V006T09A015/2476548/v006t09a015-detc2018-85232.pdf by McGill University user on 08 October 2019

Copyright © 2018 ASME

Then, we define the energy error per constraint i as the maximum of the four nonnegative energy error components $\delta e_{x_u,i}$, $\delta e_{x_l,i}$, $\delta e_{w_+,i}$, and $\delta e_{w_-,i}$

$$\delta e_i = \max\left(\delta e_{x_u,i}, \delta e_{x_l,i}, \delta e_{w_+,i}, \delta e_{w_-,i}\right). \tag{20}$$

Eq. (20) is always unit consistent since all components in the maximum function are expressed in Joule.

Figures 1 and 2 illustrate isoline plots of the unit-consistent energy error δe_i for a grid of constraint impulses $-2 \leq x_i \leq 2$ and constraint-space velocities $-2 \leq w_i \leq 2$. The thick solid blue line represents zero error $\delta e_i = 0$ and the thin solid black lines the corresponding value of δe_i . The error increases quadratically along the dashed red lines. The slope of the dashed lines is given by the tangent of the inverse effective mass element a_{ii}. Note that infinitely many parallel dashed lines can be drawn.

Finally, the total error of the system can be defined as the ℓ_1-norm

$$\delta e = ||\delta \mathbf{e}||_1 = \sum_{i=1}^{k} |\delta e_i|, \tag{21}$$

given a component vector $\delta \mathbf{e} = \left[\delta e_1 \dots \delta e_n\right]^{\mathrm{T}}$ composed of the constraint errors δe_i. We choose the ℓ_1-norm to simply add up all energy constraint errors. The units are always consistent since all components of $\delta \mathbf{e}$ carry energy units.

Computational Complexity This section outlines the computational complexity of the error measure with respect to the overall complexity of a direct solver. For direct solvers, the MLCP lead matrix $\mathbf{A}$ is explicitly formed so that its diagonal elements a_{ii} are known [14]. Furthermore, all impulse and velocity components x_i and w_i are already available since they need to be verified to satisfy the bounds. Then, the components $\delta x_{u,i}$, $\delta x_{l,i}$, $w_{+,i}$, and $w_{-,i}$ are deduced using minimum and maximum functions. The computations of $\delta e_{x_u,i}$, $\delta e_{x_l,i}$, $\delta e_{w_+,i}$, $\delta e_{w_-,i}$, and δe_i require a combination of floating point operations and min-max function. This has to be done for n variables per iteration and all variables have to be added together which leads to overall computational complexity of $\mathcal{O}(n)$. A direct solver requires a matrix factorization of complexity $\mathcal{O}(n^3)$ per iteration which can be sped up to $\mathcal{O}(bn^2)$ for banded matrices with bandwidth b. Thus, the cost of the error measure computation is negligible for the large problems.

Interpretation In Eqs. (16) and (17), the error in the impulses $\delta x_{u,i}$ or $\delta x_{l,i}$ is transformed into the upper impulse energy error $\delta e_{x_u,i}$ or the lower impulse energy error $\delta e_{x_l,i}$ by multiplication with the inverse effective mass a_{ii}. In Eqs. (18) and (19), we

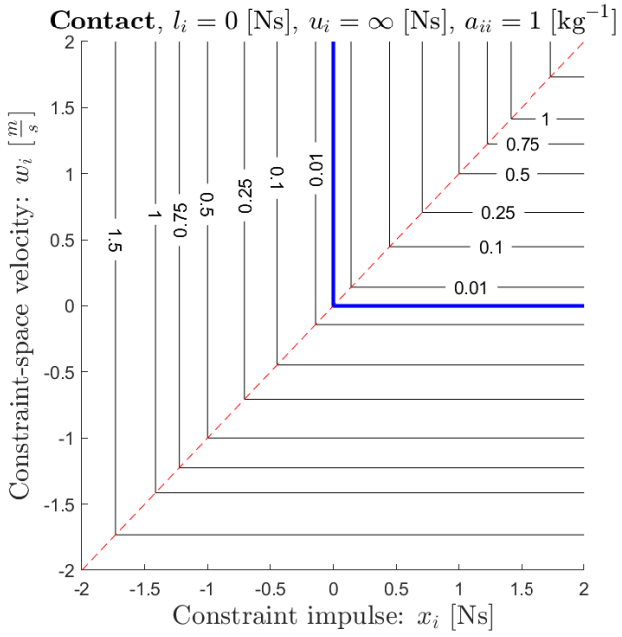

FIGURE 1. Energy error isolines for contact constraints given $a_{ii} = 1\,[\mathrm{kg}^{-1}]$ expressed in Joule. The error is zero on the thick solid blue line and increases quadratically along the dashed red lines.

determine the positive velocity energy error $\delta e_{w_+,i}$, and the negative velocity energy error $\delta e_{w_-,i}$. These two error components can only be nonzero if the constraint-space velocity w_i is nonzero so that either $w_{-,i} > 0$ or $w_{+,i} > 0$. According to Eqs. (3) and (4), nonnegative sliding velocity components $w_{+,i}$ or $w_{-,i}$ are permitted if the constraint impulse x_i equals the lower or upper bound l_i or u_i, respectively. If the MLCP solver computes an impulse greater than the upper bound u_i, i.e. $\delta x_{u,i} > 0$, or smaller than the lower bound l_i, i.e. $\delta x_{l,i} > 0$, then the impulse error is already determined in $\delta e_{x_u,i}$ or $\delta e_{x_l,i}$ and we do not need to consider $\delta x_{u,i}$ or $\delta x_{l,i}$ in the computation of $\delta e_{w_-,i}$ or $\delta e_{w_+,i}$, respectively. However, we do consider $\delta x_{l,i}$ and $\delta x_{u,i}$ in the bound saturations $\sigma_{u,i}$ and $\sigma_{l,i}$, respectively. Thus, $\delta e_{w_+,i}$ should be nonzero only if $w_{+,i} > 0$ and $\sigma_{l,i} = (x_{0,i} + \delta x_{u,i}) - l_i > 0$ simultaneously, e.g. if a body in contact slides in positive direction and the friction impulse is below the lower bound.

Let us assume that $w_{+,i} > 0$ and $\sigma_{l,i} > 0$, then we need to choose which of the two should be considered as the error. If the positive residual velocity is large $w_{+,i} \gg 0$ and the impulse is close to the lower bound $\sigma_{l,i} \approx 0$, it is more likely that the impulse should in fact be equal to the lower bound, i.e. $\sigma_{l,i} = 0$. This means that a positive component $w_{+,i}$ would not be considered as an error and the error is defined as $\{\frac{1}{2} a_{ii} \sigma_{l,i}^2\}$. Therefore, it is preferred to choose the minimum of $\{\frac{1}{2} a_{ii} \sigma_{l,i}^2\}$ and $\{\frac{1}{2a_{ii}} w_{+,i}^2\}$ to define the energy error component $\delta e_{w_+,i}$ in Eq. (18).

Downloaded from https://asmedigitalcollection.asme.org/IDETC-CIE/proceedings-pdf/IDETC-CIE2018/51838/V006T09A015/2476548/v006t09a015-detc2018-85232.pdf by McGill University user on 08 October 2019

Copyright © 2018 ASME

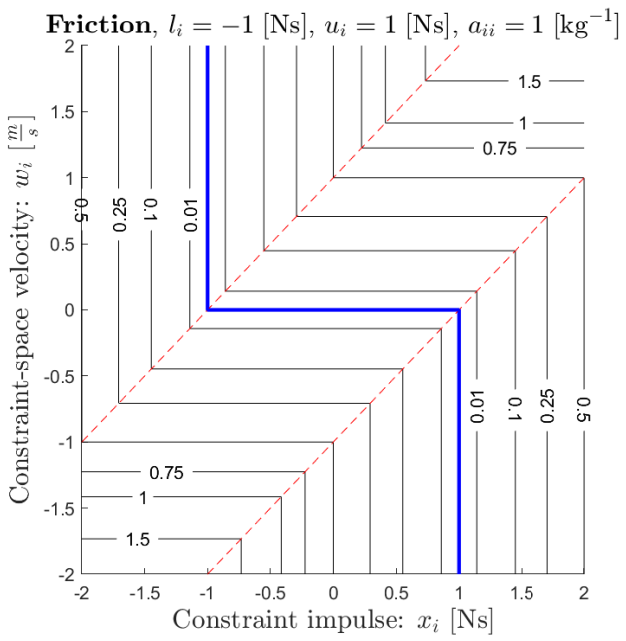

FIGURE 2. Energy error isolines for friction given $a_{ii} = 1\,[\text{kg}^{-1}]$ expressed in Joule. The error is zero on the thick solid blue line and increases quadratically along the dashed red lines.

RESULTS

In this section, we present an example for which the existing error measures in Eqs. (7) and (10) are unit inconsistent whereas the novel energy error measure in Eq. (21) obtains unit-consistent results. Furthermore, we test the existing error measures and the novel energy error measure for an iterative solver which computes solutions of MLCPs obtained from a brick wall simulation. We show that the solver error decreases continuously for the novel measure as expected for an iterative solver.

Case Study

We illustrate the unit consistency issue of the existing error measure using a discrete time, frictionless model of a rigid rod, shown in Figure 3, which is initially at rest, i.e. $\mathbf{v} = \mathbf{0}$. An external moment $T_x = 10$ Nm is applied about the centre of mass G of the $m = 1.5$ kg heavy rod which contacts the ground in two points at both ends of the rod under the effect of gravity $g = 9.81\,[\frac{\text{m}}{\text{s}^2}]$. The diameter of the rod is negligible with respect to its length of $l = 1.5$ m. The constraint Jacobian $\mathbf{J}$, the mass matrix $\mathbf{M}$, and applied forces $\mathbf{f}_a$ are determined to be

$$\mathbf{J} = \begin{bmatrix} 0 & 0 & 1 & -\frac{l}{2} & 0 & 0 \\ 0 & 0 & 1 & \frac{l}{2} & 0 & 0 \end{bmatrix}, \quad \mathbf{M} = \text{diag}\left\{ m\mathbf{E}_{3\times 3},\ \frac{1}{12}ml^2,\ I_y,\ \frac{1}{12}ml^2 \right\},$$
$$\mathbf{f}_a = \begin{bmatrix} 0 & 0 & -mg & T_x & 0 & 0 \end{bmatrix}^{\text{T}}, \tag{22}$$

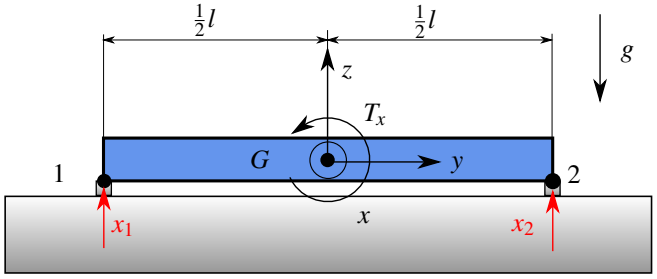

FIGURE 3. Rigid rod contacting the ground in two points

where $\mathbf{E}_{3\times 3}$ is the 3×3 identity matrix and I_y is small. We assume that the constraints are to be enforced exactly, i.e. there is no constraint relaxation. Given the time step size $h = 0.01$ s, we formulate an LCP to determine the constraint impulses $\mathbf{x} = [x_1,\, x_2]^{\text{T}}$ and constraint-space velocities $\mathbf{w} = [w_1,\, w_2]^{\text{T}}$ at the two contact points

$$\begin{bmatrix} \frac{4}{m} & -\frac{2}{m} \\ -\frac{2}{m} & \frac{4}{m} \end{bmatrix} \begin{bmatrix} x_1 \\ x_2 \end{bmatrix} + \begin{bmatrix} v_z - \frac{l}{2}\omega_x l - h\left(g + \frac{6}{ml}T_x\right) \\ v_z + \frac{l}{2}\omega_x l - h\left(g - \frac{6}{ml}T_x\right) \end{bmatrix} =$$
$$\underbrace{\begin{bmatrix} 1\,\frac{1}{\text{kg}} & -0.5\,\frac{1}{\text{kg}} \\ -0.5\,\frac{1}{\text{kg}} & 1\,\frac{1}{\text{kg}} \end{bmatrix}}_{\mathbf{A}} \underbrace{\begin{bmatrix} x_1 \\ x_2 \end{bmatrix}}_{\mathbf{x}} + \underbrace{\begin{bmatrix} -0.2981\,\frac{\text{m}}{\text{s}} \\ 0.1019\,\frac{\text{m}}{\text{s}} \end{bmatrix}}_{\mathbf{b}} = \underbrace{\begin{bmatrix} w_1 \\ w_2 \end{bmatrix}}_{\mathbf{w}},$$
$$\mathbf{0} \le \mathbf{x} \perp \mathbf{w} \ge \mathbf{0}, \tag{23}$$

where $v_z = 0\,[\frac{\text{m}}{\text{s}}]$ and $\omega_x = 0\,[\frac{1}{\text{s}}]$.

We consider a principal pivoting method [1] starting with the initial guess that the constraint impulse x_1 and the constraint-space velocity w_2 are zero. Then, it follows directly from Eq. (23) that $x_2 = -0.1019$ [Ns] and $w_1 = -0.2981\,[\frac{\text{m}}{\text{s}}]$, both of which violate the nonnegativity conditions. Physically, x_2 can be interpreted as an adhesive impulse acting in negative z-direction to prevent the contact at point 2 from detaching. This leads to a negative value for w_1 which is the resulting velocity of the rod at contact point 1 so that the rod would penetrate the ground.

The novel unit-consistent error measure can also be applied to an LCP since this is a special case of the MLCP where $\boldsymbol{l} = \mathbf{0}$ and $\mathbf{u} \to \infty$. Measuring the solver error for this scenario using the Fischer-Burmeister function in Eq. (7) results in $\delta\phi_{\text{FB}} = |\delta\phi_{\text{FB},1}| + |\delta\phi_{\text{FB},2}| = |w_1| + |x_2| = 0.2981\,[\frac{\text{m}}{\text{s}}] + 0.1019$ [Ns], where $\delta\phi_{\text{FB},1}$ and $\delta\phi_{\text{FB},2}$ are computed using Eqs. (5) and (6). We can see that $\delta\phi_{\text{FB}}$ has no physical meaning because velocity and impulse components simply cannot be added. It is apparent that this unit inconsistency also occurs if the solver error is determined using the natural residual. The unit-consistent energy error measure overcomes this issue through calculation of the energy error components equivalent to the error in w_1 and x_2. The constraint errors

Downloaded from https://asmedigitalcollection.asme.org/IDETC-CIE/proceedings-pdf/IDETC-CIE2018/51838/V006T09A015/2476548/v006t09a015-detc2018-85232.pdf by McGill University user on 08 October 2019

Copyright © 2018 ASME

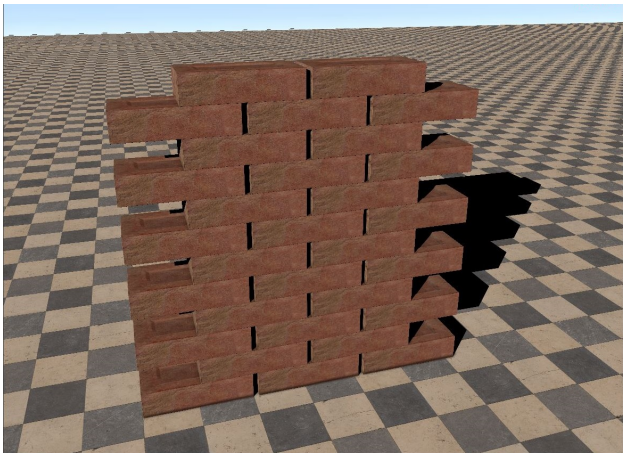

FIGURE 4. Brick wall example

measure the energy error associated with a constraint and can be determined to be $\delta e_1 = \frac{1}{2a_{11}} w_{-,1}^2 = 4.44 \cdot 10^{-2}$ [J] and $\delta e_2 = \frac{1}{2} a_{22} \delta x_{l,2}^2 = 5.2 \cdot 10^{-3}$ [J] using Eqs. (16) to (20). Now, we can compute a unit-consistent system error $\delta e = \delta e_1 + \delta e_2 = 4.96 \cdot 10^{-2}$ [J] using Eq. (21).

Simulation Results

We test the novel energy error measure for the example in Figure 4 which consists of a stack of 30 boxes laid out in a brick wall pattern. The brick wall is 12 bricks tall, and we alternate between rows of two or three bricks in width. Furthermore, there are small lateral gaps between two adjacent bricks. We use a direct solver to accurately simulate the wall behavior and store an MLCP for each of the 500 time steps. Then, the projected Gauss-Seidel (PGS) iterative method is used to find a solution of the different MLCPs with 100 solver iterations for each time step. Iterative solvers are known to converge to a solution by continuously improving the solution with every iteration. Hence, we expect the error to decrease with the number of iterations. Note that it is possible that iterative solvers do not converge to the solution. This depends on the physical problem and the mathematical properties of the MLCP lead matrix. Convergence is guaranteed only if the spectral radius of matrix $\mathbf{A}$ is smaller than one.

Figure 5 shows the results for the solver error per iteration defined by the Fischer-Burmeister error measure $\delta\phi_{\mathrm{FB}}$, the natural residual error measure $\delta\phi_{\mathrm{res}}$, and the energy error measure δe. Only the latter treats physical units consistently. The set of results contains the solver error per iteration for $\bar{T} = 500$ time steps for which we compute the average error and the standard deviation. The average energy error per time step μ_{e} is defined as

$$\mu_{\mathrm{e}} = \frac{1}{\bar{T}} \left(\sum_{k=1}^{\bar{T}} \delta e\,(t_k) \right), \tag{24}$$

where $\delta e\,(t_k)$ is the energy error at time t_k, and the standard deviation of the energy error σ_{e} is given as

$$\sigma_{\mathrm{e}} = \sqrt{\frac{1}{\bar{T}-1} \left(\sum_{k=1}^{\bar{T}} \{\delta e\,(t_k) - \mu_e\}^2 \right)}. \tag{25}$$

The average and standard deviation for the Fischer-Burmeister and natural residual solver errors can also be calculated using this approach by replacing $\delta e\,(t_k)$ by the respective error $\delta\phi_{\mathrm{FB}}\,(t_k)$ and $\delta\phi_{\mathrm{res}}\,(t_k)$ at time t_k.

The three plots on the right of Figure 5 show the iteration-error curves for all 500 time steps. The three plots on the left illustrate the average values of the solver error μ_{FB}, μ_{res}, and μ_{e} as well as the upper and lower error limits given by the average plus or minus the standard deviation of the solver error $\mu_{\mathrm{FB}} \pm \sigma_{\mathrm{FB}}$, $\mu_{\mathrm{res}} \pm \sigma_{\mathrm{res}}$, and $\mu_{\mathrm{e}} \pm \sigma_{\mathrm{e}}$. The latter visualizes the amount of variation of the solver errors over the time steps. The small vertical gap between the averages μ_{FB}, μ_{res}, as well as μ_{e} and the upper and lower limits $\mu_{\mathrm{FB}} \pm \sigma_{\mathrm{FB}}$, $\mu_{\mathrm{res}} \pm \sigma_{\mathrm{res}}$, as well as $\mu_{\mathrm{e}} \pm \sigma_{\mathrm{e}}$ indicates that the variation of the solver errors is relatively small for the different time steps as expected for a motionless example. For the error curves of the Fischer-Burmeister and the natural residual error measures, the solver error increases in the first ten iterations, reaches a maximum, and then it decreases exponentially with the iteration count. The error curves for the energy error measure do not show any error increase in the first ten iterations which is more realistic for a convergent iterative solver. Moreover, the exponential decay is steeper than for the other error measures. This is apparent since the energy error decreases quadratically with w_i and x_i whereas the Fischer-Burmeister and the natural residual error descend linearly with w_i and x_i.

On the right of Figure 5, we observe that all error curves start from similar error values which then diverge from each other with an increasing number of iterations. The iterative PGS solver is initialized with the same value $\boldsymbol{\lambda} = \mathbf{0}$ for all time steps, i.e. it is not warm started using the solution of the last time step. Thus, the error value is similar in the first iteration of each time step before it converges toward zero at varying rates. The presented error measure does not intend to capture all error sources in the simulation but only the error due to the MLCP solver. Note that the accuracy level obtained by the PGS solver would not be sufficient to keep the brick wall permanently stable. It would take several thousand iterations to maintain stability long term. However, the objective of this example is not to present accurate simulation results for the stable brick wall simulation but merely to show that the solver error decreases with the iteration count for the novel unit-consistent measure.

Downloaded from https://asmedigitalcollection.asme.org/IDETC-CIE/proceedings-pdf/IDETC-CIE2018/51838/V006T09A015/2476548/v006t09a015-detc2018-85232.pdf by McGill University user on 08 October 2019

Copyright © 2018 ASME

DISCUSSION

Figure 5 shows that the energy error decreases when the solver converges to the solution of the MLCP. The energy error measure behaves qualitatively similar to the Fischer-Burmeister and the natural residual error, except for the first ten iterations where only the energy error shows the expected decay. We have shown that only the energy error measure computes the solver error in a unit consistent manner and it reaches zero error if and only if a valid solution to the MLCP is found. The unit-consistent measure does not require any reference solution which is a major advantage since it can be costly to compute a reference for large-scale problems.

Moreover, the cost of computing the energy error does not significantly impact the overall MLCP solution algorithm performance for direct solvers even if the error is obtained in every iteration. Thus, the computation can be done for real-time simulations without affecting the performance noticeably. If a direct solver is not able to terminate due to a time constraint, we can monitor all the iterations and determine the solution with the least energy error, and use this solution for further calculations. This would allow us to obtain a better solution and possibly improve the numerical stability.

CONCLUSION

The most used error measures for MLCP solvers do not take the physical nature of mechanical models into account, which leads to an inconsistent treatment of units. The proposed unit-consistent error measure defines an energy error per constraint by means of the effective mass, which solves the unit consistency issue through the transformation of impulse and velocity errors into energy errors. Furthermore, simulation results illustrate that the energy error decreases monotonically when the MLCP solver converges to the solution. The computational cost of the novel error measure is inexpensive in comparison to the overall cost of an MLCP solver iteration of direct solvers.

As future work, the unit-consistent error could be used to stop the MLCP solver if a solution of the MLCP is found which is close enough to the true solution. This requires the definition of an error threshold which classifies what solution will be considered as close enough to the the true one and which therefore affects the solution accuracy. It is particularly challenging since the required accuracy of a solution depends on the engineering application and the simulation scenario.

REFERENCES

[1] Júdice, J. J., 1994. "Algorithms for linear complementarity problems". In *Algorithms for Continuous Optimization*, E. G. Spedicato, ed. Springer, pp. 435–474.

[2] Pang, J.-S., 1997. "Error bounds in mathematical programming". *Mathematical Programming,* ***79***(1-3), pp. 299–332.

[3] Fukushima, M., 1996. "Merit functions for variational inequality and complementarity problems". In *Nonlinear Optimization and Applications*, G. D. Pillo and F. Giannessi, eds. Springer, pp. 155–170.

[4] Pang, J.-S., 1986. "Inexact newton methods for the nonlinear complementarity problem". *Mathematical Programming,* ***36***(1), pp. 54–71.

[5] Lacoursière, C., Lu, Y., Williams, J., and Trinkle, J., 2013. "Standard interface for data analysis of solvers in multibody dynamics". In Canadian Conference on Nonlinear Solid Mechanics.

[6] Williams, J., Lu, Y., Niebe, S., Andersen, M., Erleben, K., and Trinkle, J. C., 2013. "RPI-MATLAB-Simulator: A tool for efficient research and practical teaching in multibody dynamics". In Workshop in Virtual Reality Interactions and Physical Simulation, pp. 71–80.

[7] Lu, Y., and Trinkle, J., 2015. "Comparison of multibody dynamics solver performance: Synthetic versus realistic data". In ASME International Design Engineering Technical Conferences and Computers and Information in Engineering Conference, pp. 1–10.

[8] Lacoursière, C., Linde, M., Lu, Y., and Trinkle, J., 2015. "A framework for data exchange and benchmarking of frictional contact solvers in multibody dynamics". In ECCOMAS Thematic Conference on Multibody Dynamics, pp. 2–3.

[9] Lacoursière, C., 2006. A regularized time stepper for multibody systems. Tech. rep., Umeå University, Sweden, HPC2N and Department of Computing Science.

[10] Silcowitz, M., Niebe, S., and Erleben, K., 2009. "Nonsmooth newton method for fischer function reformulation of contact force problems for interactive rigid body simulation". In Workshop in Virtual Reality Interactions and Physical Simulation, pp. 105–114.

[11] Lu, Y., Williams, J., Trinkle, J., and Lacoursiere, C., 2014. "A framework for problem standardization and algorithm comparison in multibody system". In ASME International Design Engineering Technical Conferences and Computers and Information in Engineering Conference, pp. 1–10.

[12] Khatib, O., 1995. "Inertial properties in robotic manipulation: An object-level framework". *The International Journal of Robotics Research,* ***14***(1), pp. 19–36.

[13] Kövecses, J., 2008. "Dynamics of mechanical systems and the generalized free-body diagram, part 1: General formulation". *ASME Journal of Applied Mechanics,* ***75***(6), pp. 1–12.

[14] Júdice, J. J., and Pires, F. M., 1994. "A block principal pivoting algorithm for large-scale strictly monotone linear complementarity problems". *Computers & Operations Research,* ***21***(5), pp. 587–596.

Downloaded from https://asmedigitalcollection.asme.org/IDETC-CIE/proceedings-pdf/IDETC-CIE2018/51838/V006T09A015/2476548/v006t09a015-detc2018-85232.pdf by McGill University user on 08 October 2019

Copyright © 2018 ASME

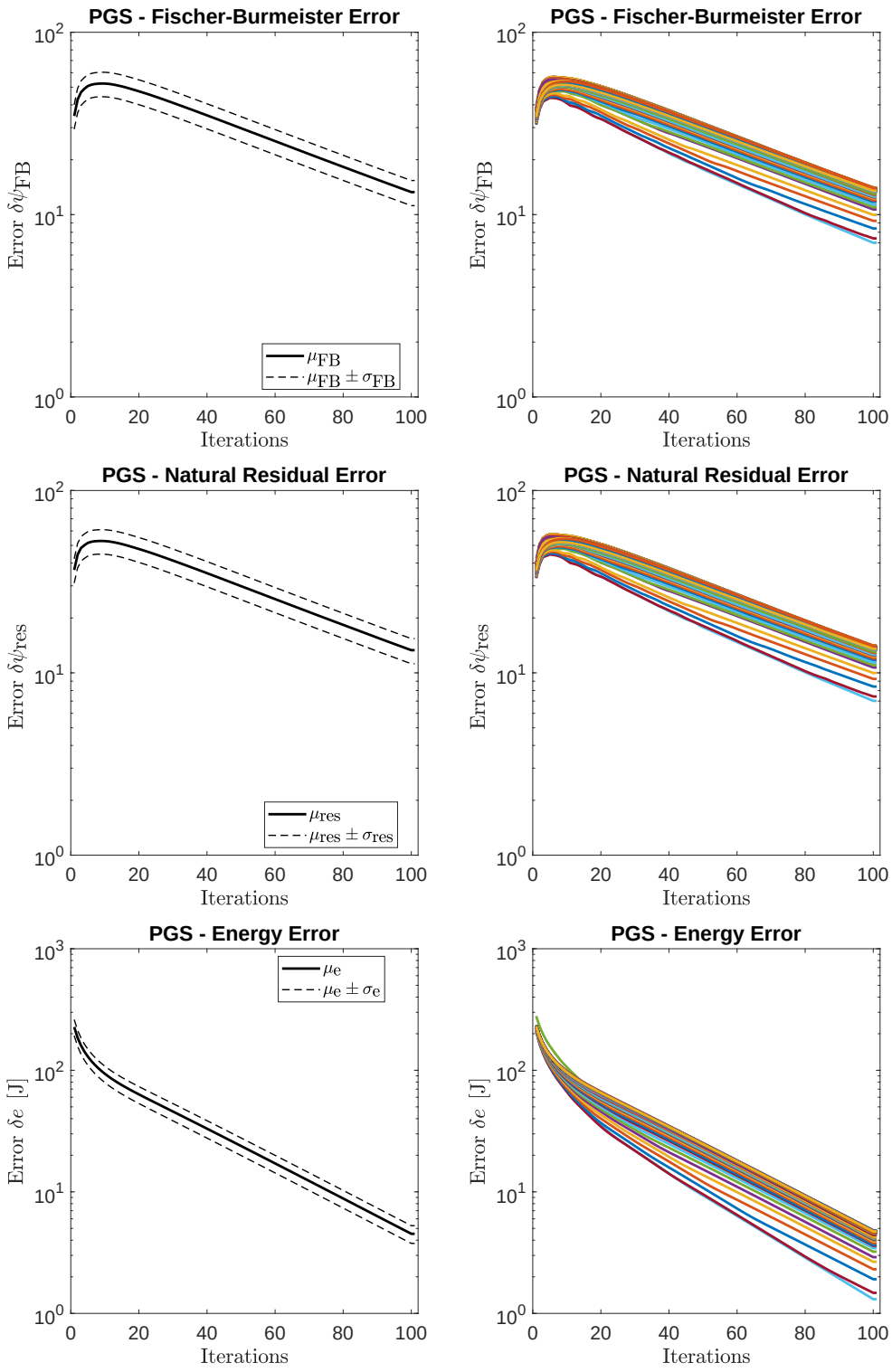

FIGURE 5. Brick wall example in Figure 4 solved by PGS, on the left solid lines illustrate the average errors and the dashed lines the upper and lower error limit given by the average plus or minus the standard deviation, on the right each line represents the iteration-error curve for one time step

Downloaded from https://asmedigitalcollection.asme.org/IDETC-CIE/proceedings-pdf/IDETC-CIE2018/51838/V006T09A015/2476548/v006t09a015-detc2018-85232.pdf by McGill University user on 08 October 2019

Copyright © 2018 ASME